Vibrational Mean Free Paths and Thermal Conductivity Accumulation Functions for Amorphous Materials

Jason M. Larkin[1] and Alan J. H. McGaughey[1]

[1]*Department of Mechanical Engineering*

Carnegie Mellon University

Pittsburgh, PA 15213

(Dated: July 11, 2013)

Abstract

BEGINALAN

Understanding thermal transport in crystalline systems requires detailed knowledge of phonons, which are the quanta of energy associated with atomic vibrations. By definition, phonons are non-localized vibrations that transport energy over distances much larger than the atomic spacing. For disordered materials (e.g., alloys, amorphous phases), with the exception of very long-wavelength (low-frequency) modes, the vibrational modes are localized and do not propagate like phonons. The film thickness and temperature dependence of thermal conductivity measured by experiments show indirectly that propagating modes contribute significantly for a-Si but not a-SiO2, with contribution from vibrational modes with large mean free paths (100-1000 nm). Recent measurements using a broadband FDTR technique argue that these vibrational mean free paths can be probed by varying the penetration depth to measure the thermal conductivity accumulation function. Using lattice dynamics calculations and molecular dynamics simulations on realistic models of a-SiO2 and a-Si, we predict and characterize the contributions from phonons and localized vibrations to vibrational thermal conductivity. The vibrational mean free paths are predicted for these two amorphous materials and the thermal conductivity accumulation function is compared with experimental results, particularly from Regner et al.

ENDALAN

I. INTRODUCTION

BEGINALAN

Amorphous silicon (a-Si) and nanocrystalline silicon have applications in high-efficiency solar cells.(cite) Films and substrates made of a-SiO2 and a-Si have wide application. (cite) Understanding the thermal transport in these amorphous systems is critical to improving their performance. Thermal transport at scales comparable to phonon wave- lengths and mean free paths (MFPs) is presently a topic of considerable interest.[1–4] Recently, nanostructured materials such as nanowires, superlattices, and composites with strongly reduced thermal conductivities due to phonon scattering at interfaces and boundaries have been reported and are being considered for use in thermoelectric applications.[3–6] Recent empirical and first-principles calculations show that MFPs of phonons relevant to thermal conductivity vary by more than 5 orders of magnitude in crystalline materials.[7] Traditionally, empirical expressions and simple relaxation time models have been the only means to estimate MFPs.[8]

Experimentally, inelastic neutron scattering has been used to measure phonon lifetimes in certain materials, but this technique is more suited for single crystal samples.[9] Koh et al. proposed a time-domain thermal reflectance (TDTR) technique which uses a variation of modulation frequency to measure MFPs, but this technique is limited by the modulation frequency.[10] An x-ray diffraction and thermoreflectance technique can measure ballistic transport in some structures.[11] The thermal conductivity accumulation function can be predicted for bulk crystalline systems using TDTR and frequency-domain thermal reflectance (FDTR) techniques. (cite) The understanding of the accumulation function for bulk crystalline is understood fairly well experimentally[12] and theoretically.[13] However, understanding of the accumulation in amorphous systems is still not well understood.[14–19] Recent measurements by Regner using broadband FDTR argue that the thermal conductivity accumulation function can be measured by varying the penetration depth of the experimental measurement.[20]

Experimental measurements of the thermal conductivity of thin films of a-SiO2 and a-Si at varying temperatures gives indirect information about the low-frequency, propagating modes.(cite) For a-SiO2, varying temperature and film thickness[21,22] measurements all suggest that the propagating modes contribute a negligible amount to thermal conductivity.

However, the behavior of the low-frequency modes has only recently been understood by experimental measurements,[23–27] where a cross-over of the low-frequency scaling of the vibrational lifetimes from Rayleigh (quartic)(cite) to Umklapp (quadratic)(cite) is observed.

For a-Si the low-frequency behavior is less understood. Temperature varying(cite) and film thickness-varying measurements[15,17,18,28–32] suggest multiple and different behavior of the low-frequency scaling of the mean free paths of vibrational modes in a-Si. Comparison of experimental measurements by Pompe[33] and Cahill[15,34] show a plateau of thermal conductivity with temperature, which can be predicted by the the model from FKAW which assumes a ω^{-4} scaling.[14] Low temperature conductivity and specific heat measurements demonstrate that the propagating modes in a-Si and doped a-Si follow $\Lambda \propto \omega^{-2}$,[30,35] where no thermal conductivity plateau is observed[18,30,35] There is a clear film thickness t_f dependence of the thermal conductivity of a-Si, particularly for $t_f > 10$ μm, (cite) where conductivities of $1.4 - 6$ W/m-K have been reported. (cite) Both quadratic[16] and quartic[14,18**?**] scalings of the low-frequency MFPs have been considered to explain these experimental measurements. More experimental measurements are needed to understand the low-frequency behavior in a-Si thin films.(cite)

Low temperature conductivity and specific heat measurements demonstrate that the propagating modes in a-Si and doped a-Si follow $\Lambda \propto \omega^{-2}$.[30,35] Comparison of experimental measurements by Pompe[33] and Cahill[15,34] show a plateau of thermal conductivity with temperature, which can be predicted by the the theory from FKAW which assumes a ω^{-4} scaling.[14] Zink et al. measured the thermal conductivity of e-beam evaporated amorphous silicon thin films over a wide tem- perature range and found now plateau, which is predicted from the FAB theory and an ω^{-2} scaling.[16]

In this work, we perform Molecular Dynamics (MD) simulations and Lattice Dynamics calculations on large models of a-SiO2 and a-Si. The results are used to understand recent experimental measurements using a broadband frequency domain thermal reflectance (FDTR) technique with varying penetration depths L_p.[20] Large MD simulations of models for a-SiO2 show (within the errors) no dependence on the system size, indicating that propagating modes do not make a significant contribution to thermal conductivity. This is confirmed by modal analysis, which demonstrates that propagating modes contribute a negligible amount to thermal conductivity. At low frequency, a quadratic scaling of the vibrational mode lifetimes is a reasonable fit to the predictions, in agreement with previous

models of a-SiO2.(cite)

We predict the thermal conductivity of bulk a-Si using (to our knowledge) the largest MD simulation for a model of a-Si.(cite) Scaling of thermal conductivity with system size indicates that the low-frequency propagating modes in bulk a-Si follow a Debye-like model with a quadratic scaling of the mode lifetime with frequency. (cite) A modal analysis of a large a-Si model supports the evidence for quadratic scaling of lifetimes at low frequency, which is not definitive using the AF diffuson theory.[14,16] The propagating modes are found to contribute significantly to the thermal conductivity of a-Si an amount similar to that predicted by other models of a-Si.(cite)

The spectrum of vibrational MFPs and the accumulated thermal conductivity (cite) are predicted for a-SiO2 and a-Si. The thermal conductivity for our model of a-SiO2 accumulates within 95% of its bulk value for vibrational mean free paths (MFPs) < 10 nm. This result explains the experimental measurements of Regner et al, which show no measured dependence of the thermal conductivity on L_p,[20] and experimental measurements of the thermal conductivity of thin films which show no dependence on film thickness.(cite)

Using a simple boundary scattering model, the accumulated thermal conductivity of a-Si thin films are predicted from our model of bulk a-Si. The predicted accumulated thermal conductivity reproduces the experimentally measured penetration depth-dependent thermal conductivity qualitatively.(cite) We consider both quadratic and quartic scalings of the low-frequency vibrational lifetimes. By considering both scalings, our model of thin-film a-Si thermal conductivity accumulation can span the range of the lower(cite) and higher[17,18] experimentally measured thermal conductivity of varying thickness a-Si thin films.

The predicted contribution to thermal conductivity of non-propagating modes from our model of a-Si is in good agreement with the plateau of accumulated thermal conductivity from broadband FTDR. The quadratic scaling of low-frequency mode lifetimes does not predict the steep dependence of thermal conductivity on L_p, while the quartic scaling can qualitatively. Given the lack of experimental measurements of the low-frequency scaling of vibrational mode lifetimes,(cite) low-temperature broadband FDTR measurements can help to show which scaling, quadratic or quartic, is present in a-Si thin films with varying deposition technique. The results could answer the question of whether quartic versus quadratic scaling is responsible for the large thickness variation of the thermal conductivity of a-Si thin films.

II. THEORETICAL FORMULATION

A. Vibrational Thermal Conductivity

To calculate the total vibrational thermal conductivity k_{vib} of amorphous solids, we predict the contributions from k_{pr} and k_{AF},

$$k_{vib} = k_{pr} + k_{AF}, \tag{1}$$

where k_{pr}[36–38] is the contribution from phonon-like propagating modes and k_{AF} is the non-propagating contribution from the Allen-Feldman (AF) theory of diffusons.[14] The form of Eq. (1) has been used in several previous studies with varying assumptions. The various assumptions all lead to predictions that k_{pr} is an negligible ($< 10\%$) and non-negligible ($> 20\%$) fraction of k_{vib} for a-SiO2(cite) and a-Si(cite), respectively.

We predict the contribution k_{pr} using a Debye-like model,(cite)

$$k_{pr} = \frac{1}{V}\int_0^{\omega_{cut}} d\omega DOS(\omega)C(\omega)D_{pr}(\omega), \tag{2}$$

where V is the system volume, ω is the vibrational mode frequency, $DOS(\omega)$ is the vibrational density of states, $C(\omega)$ is the vibrational mode specific heat, ω_{cut} identifies the transition to propagating modes (see Section), and $D_{pr}(\omega)$ is the propagating mode thermal diffusivity. The cut-off frequency ω_{cut} identifies the transition from propagating (phonon-like) to non-propagating (diffuson) modes (see Section).[14–18] The propagating contribution k_{pr} is written as an integral because the finite simulation sizes studied in this work (and others)[14,16] limit the lowest frequency vibrational modes which can be studied. Eq. (2) can be obtained using the single-mode relaxation time approximation to solve the Boltzmann transport equation for a phonon gas.[38]. Assumed in Eq. (2) are isotropy (valid for an amorphous material) and a single phonon polarization,(cite) making the properties a function of the mode frequency ω only. The choice of a single phonon polarization (i.e., an averaging of the transverse and longitudinal branches)(cite) does not significantly change the results predicted in this work, or others.[14–18,24]

Under the Debye approximation, which assumes isotropic and linear dispersion (i.e., $v_g = v_s$), the density of states, $DOS(\omega)$, is

$$DOS(\omega) = \frac{3\pi\omega^2}{2v_{s,DOS}^3}, \tag{3}$$

where v_s is an appropriate sound speed.(cite) Since we use MD simulations, which are classical and obey Maxwell-Boltzmann statistics,[39] we take the phonon and diffuson specific heat to be $C(\omega) = k_\mathrm{B}$ in the harmonic limit. This harmonic approximation has been shown to be valid for a-Si modeled using the Stillinger-Weber potential at the temperatures of interest here for low-frequency modes (see Section).(cite) Taking the classical limit for the specific heat allows for a direct comparison between the MD- and lattice dynamics-based methods.

In a disordered system, only the diffusivitiy of the low-frequency propagating modes can be written as(cite)

$$D_{pr}(\omega) = \frac{1}{3}v_g^2(\omega)\tau(\omega), \tag{4}$$

where the mode group velocity $v_g(\omega) = v_s$ and $\tau(\omega)$ is the mode lifetime. The physical picture is of propagating plane waves which travel with velocity v_s for a time τ before scattering. An equivalent physical picture in terms of a scattering length is

$$D(\omega) = \frac{1}{3}v_g(\omega)\Lambda(\omega), \tag{5}$$

where Λ is the phonon mean free path (MFP), defined as

$$\Lambda(\omega) = v_g(\omega)\tau(\omega). \tag{6}$$

In a disordered system, is only valid in the low-frequency, long-wavelength limit.(cite) Because Eq. (4) is only valid at low frequencies, the mode diffusivity D is the fundamental quantity for modes at all frequencies.(cite) The propagating thermal diffusivity is modeled using

$$D_{pr}(\omega) = B\omega^{-n}, \tag{7}$$

where B and n are constants. At low frequencies (long wavelengths), $v_g = v_s$ and the scaling of diffusivity with frequency comes from the lifetime,

$$\tau(\omega) = B_\tau\omega^{-n}, \tag{8}$$

where $B_\tau = B/v_s^2$. For amorphous materials, the scaling exponent has been found to be $2 \geq n \leq 4$,(cite) where $n = 2$ corresponds to Umklapp scattering[40] and $n = 4$ is Rayleigh scattering from point defects in a crystal.[41] The form of the $DOS(\omega)$ [Eq. (3)] and $D(\omega)$ [Eq. (7)] with $n \leq 2$ ensures that the thermal conductivity Eq. (2) is finite.(cite) The form for $D(\omega)$ [Eq. (**??**)] with $n > 2$ causes the thermal conductivity [Eq. (2)] to diverge in the low-frequency limit as the system size is increased,(cite) which can be fixed using additional anharmonic scattering[14,16] or boundary scattering.[17**?** ,18]

For non-propagating modes in the AF diffuson theory, $D(\omega)$ cannot be written as Eq. (4).[42] The diffuson contribution to thermal conductivity, k_{AF}, is[14,16]

$$k_{AF} = \frac{1}{V} \sum_{\omega_i > \omega_{cut}} C_i(\omega) D_{AF,i}(\omega), \tag{9}$$

where ω_i is the frequency of the ith diffuson mode, $C_i(\omega_i)$ is the diffuson specific heat, and $D_{AF,i}$ is the diffuson diffusivity. Eq. (9) is written as a sum because there are enough high-frequency diffuson modes in the finite-size systems studied in this work (and others).[14,16] Written as an integral, Eq. (**??**) has the same form as Eq. 2, which can be derived starting with the Kubo theory[18,24,42–44] and taking the limit of zero phonon self-energy.[24] The AF diffusivities are predicted by[42]

$$D_{AF,i} = \frac{\pi V^2}{\hbar^2 \omega_i^2} \sum_{j \neq i} |S_{ij}|^2 \delta(\omega_i - \omega_j) \tag{10}$$

where $\hbar$ is Planck's constant, S_{ij} is the heat current operator between vibrational modes i and j, and δ is the Dirac delta function. The diffusivity of diffusons can be calculated from harmonic lattice dynamics theory.[14,16,42] The heat current opreator S_{ij} measures the thermal coupling between modes i and j based on their frequencies and spatial overlap of eigenvectors (see Section and). For Eq. (10), S_{ij} is directionally averaged because the amorphous materials studied in this work are isotropic The diffuson specific heat is taken to be $C_i(\omega) = k_\mathrm{B}$ to remain consistent with the same assumption for low-frequency propagating modes and the MD- and LD-based methods compared in this work. The implication of this assumption is discussed in Section .

B. Thermal Conductivity and Diffusivity Limits

To understand the contribution k_{AF}, it is useful to consider a high-scatter limit for the mode diffusivity,

$$D_{HS} = \frac{1}{3} v_s a, \tag{11}$$

where it is assumed that all vibrational modes travel with the sound speed v_s, and scatter over a distance of the lattice constant, a. This diffusivity assumption leads to a high-scatter (HS) limit of thermal conductivity in the classical limit[45]

$$k_{HS} = \frac{k_{\mathrm{B}}}{V_b} b v_s a, \tag{12}$$

where V_b is the volume of the unit cell and b is the number of atoms in the unit cell.[46] The advantage of k_{HS} is a simple functional form of the macroscopic material properties which can be evaluated with experimental measurements or modeling predictions. While Eqs. (11) and (12) are commonly used to establish a high-scatter limit for diffusivity and thermal conductivity, predictions for a-SiGe alloys[14] and experiments demonstrate that these are not true high-scatter limits. However, k_{HS} is a good lower limit for the thermal conductivity of a-SiO2(cite) and a-Si, as well as other glasses.(cite)

It was demonstrated by Kittel that the thermal conductivity of glasses in the high-temperature limit could be interpreted using a temperature-independent high-scatter diffusivity on the order of Eq. (11).[47] This corresponds to a propagating (phonon) model with MFP $\Lambda = a$, too small to justify use of the model. The success of Kittel's theory implies that the dominant modes in most glasses are diffusons and not phonons,(cite) and $k_{vib} \approx k_{AF} = k_{HS}$. For example, amorphous Lennard-Jones argon is dominated by high-scatter modes,[48] as is a model of a-GeTe,[49] and both their $k_{vib} \approx k_{HS}$. For a-SiO_2, $k_{vib} \approx 2k_{HS}$, while it is unclear what the appropriate lattice constant a should be, making a factor of 2 reasonably uncertain.(cite) For a-Si, the experimentally measured thermal conductivity at 300 K is $k_{vib} \approx (1-6)k_{HS}$,[46] indicating that there may be a large contribution from k_{pr}.

The relative contributions of k_{pr} and k_{AF} to k_{vib} have been estimated from experiments and modeling for a-Si and a-SiO2. At 300 K for a-Si modeled by the Tersoff potential, $k_{ph} \approx k_{AF}$.[50] Earlier studies using different models of a-Si find that k_{pr} is less than half of k_{vib}.[14,16] Estimates based on experimental measurements have shown k_{pr} as low as 20%[15,16] and as

high as 80% k_{vib}.[17,18] While different predictions for a-Si depend on the experimental sample preparations (cite) and the assumed scaling of the low-frequency vibrational diffusivities (see Section and)(cite), all evidence supports that k_{pr} is a significant fraction of k_{vib}.(cite) For a-SiO2, modeling based on experiments show that k_{pr} is less than 10% of k_{vib}.(cite)

Recent broadband FDTR experiments by Regner et al. measured the apprent thermal conductivity change with frequency of a-Si and a-SiO2. By varying the FDTR frequency, the penetration depth of the experiments L_p was varied between 40 nm and 1μm.(cite) They argue that the apparent thermal conducvitiy variation with L_p represent the accumulated thermal conductivity for propagating modes with MFP less than L_p. While predictions for k_{vib}, k_{pr}, and k_{AF} have been made for a-SiO2 and a-Si,(cite) no thermal conductivity accumulation functions have been predicted to compare with Regner. Using lattice dynamics calculations and molecular dynamics simulations of large-scale (4000 atom models), we predict the inputs to Eq. (1) in Sections IV A, IV C, IV E, and the bulk thermal conductivity k_{vib} and its contributions k_{pr} and k_{AF} in Section using the mode-by-mode properties. Using very large-scale ($10,000$ to $1,000,000$ atoms) MD simulations, we predit the thermal thermal conductivity k_{vib} of bulk a-SiO2 and a-Si to compare with the predictions based on the mode-by-mode properties. For the first time, the MFPs of propagating modes in bulk a-SiO2 and a-Si are used with a boundary scattering model to predict the thermal conductivity accumulation, which is and compared with experimental thin film measurements and broadband FDTR measurements of a-SiO2 and a-Si in Section V B.

III. CALCULATION DETAILS

A. Sample Preparation

The a-SiO_2 samples are used from Ref. 51 and have size $N_a = 288$, 576, and 972. These samples were originally prepared using a melt-quench technique.(footnote) Using the same procedure, larger systems of N_a = 2880, 4608, and 34,562 were created. For the largest sample with $N_a = 34,562$ the box size $L = 8.052$ nm. All samples were simulated at a density $\rho = 2350$ kg/m^3.(cite) The atomic potential used for a-SiO_2 is the modified BKS potential from Ref. 51 except the 24-6 Lennard-Jones (LJ) potential is changed to a 12-6, which has a negligible effect on the predictions presented in this paper. The LJ potentials

use a cutoff of 8.5 $\mathring{A}$ and the Buckingham potential uses a cutoff of 10 $\mathring{A}$. The electrostatic interactions are handled using the Wolf method with exponential parameter $\eta = 0.223\mathring{A}^{-1}$ and a cutoff of 12 $\mathring{A}$.[52]

For a-Si, we use models created by the modified Wooten-Winer-Weaire (WWW) algorithm from Ref. 53. Sample sizes with N_a = 216, 1000, 4096, and 100,000 were provided, where N_a are the number of atoms in the disordered supercell. A large sample was created from the $N_a = 100,000$ sample by treating it as a unit cell and tiling twice in all directions to create an $N_a = 800,000$ sample with box size L = 24.81 nm. All a-Si structures used have $\rho = 2330$ kg/m^3, equivalent to the perfect crystal with a lattice constant of a =5.43 $\mathring{A}$. The Stillinger-Weber potential is used with these samples.[54]

Small samples of a-SiO2 and a-Si are shown in Fig. 1. Both a-SiO2 and a-Si samples were annealed at a temperature of 1100 K for 10 ns to remove meta-stability.[16] Amorphous materials have many different atomic (potential energy) configurations with nearly equivalent energies.[16,55,56] The removal of meta-stability is demonstrated by a decrease of the sample's potential energy from the pre-annealed configuration. This meta-stability can cause errors when predicting vibrational lifetimes using Normal Mode Decomposition (NMD, see Section IV D).(cite)

(footnote) The entire melt-quench procedure is performed at constant volume.[51] Crystalline silica (c-SiO2) is first melted at a temperature of 10,000 K in a cubic simulation cell at constant volume. The liquid is then quenched instantaneously to 300 K and annealed for 10 ns.

B. Simulation Details

Molecular dynamics (MD) simulations are performed using the disordered a-SiO_2 and a-Si supercells described in Section III A. The MD simulations were performed using LAMMPS[58] with time steps of dt = 0.00905 (0.0005) ps for a-SiO_2(a-Si). Ten MD simulations with different initial conditions were run and the predictions from these simulations were ensemble averaged. All MD simulations are first equilibrated in a NVT (con- stant number of atoms, volume, and temperature) ensemble for 10^6 time steps. Data are then collected from simulations in the NVE (constant number of atoms, volume, and total energy) ensemble for 2^21 time steps and the atomic trajectories sampled ever 2^8 time steps.

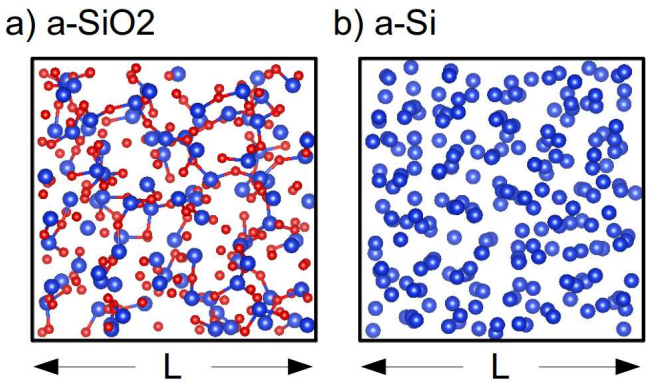

FIG. 1: (a) a sample supercell of a-SiO2 with $N_a = 288$ and cell length $L = 1.597$ nm. Samples up to size $N_a = 4,608(36,864)$ and $L = 4.026(8.052)$ nm are used for the LD(MD)-based methods in Sections and . The samples were prepared using (b) a sample supercell of a-Si with $N_a = 216$ and cell length $L = 1.597$ nm. Samples up to size $N_a = 4,096(800,000)$ and $L = 4.344(24.81)$ nm are used for the LD(MD)-based methods in Sections and . The a-Si samples were prepared using a modified WWW algorithm (see Section). Both a-SiO2 and a-Si structures are visualized using the VESTA package.[57]

The Green-Kubo (GK) method is used to predict the thermal conductivity k_{GK} (see Section) from MD simulations of the largest supercells of a-SiO2 and a-Si (see Section). The k_{GK} is predicted by window averaging the integral of the heat current autocorrelation function (HCACF).(cite) For a-SiO_2 and s-Si, a interval of the the HCACF integral can be found which is constant within the statistical noise.(cite) Similar k_{GK} (within the errors) are predicted using the first avalanche method.(cite) For $N_a = 4,608(4,096)$, the trajectories from the MD simulations used for the GK method are also used with the NMD method to predict the vibrational mode lifetimes of a-SiO2(a-Si) (Section IV D).

For the amorphous supercells studied, the only allowed wave vector is the gamma-point (i.e., $\boldsymbol{\kappa} = 0$), where $\boldsymbol{\kappa}$ is the wavevector and there are $3N_a$ polarization branches labeled by ν. Calculation of the vibrational modes at the Gamma point (referred to as Gamma modes) require the eigenvalue solution of a dynamical matrix of size $(3N_a)^2$ that scales as $[(3N_a)^2]^3$, limiting the system sizes that can be considered to $N_a = 4,608(4,096)$ for a-SiO_2(a-Si). The eigenvalue solution is required to predict the vibrational density of states (DOS (see Section), structure factors (see Section), perform the NMD technique (see Section IV D) and perform the AF calculations (see Section IV E). The frequencies and eigenvectors were

computed using harmonic lattice dynamics calculations and GULP.[52] The calculation of the AF diffuson thermal diffusivities (Eq. (10)) is performed using GULP and a Lorentzian broadening of $14\delta\omega_{avg}(5\delta\omega_{avg})$ for a-SiO^2(a-Si), where $\delta\omega_{avg}$ is the average mode frequency spacing ($\delta\omega_{avg} =$ () for a-SiO2(a-Si)). (cite) For a-Si the broadening is within 20% of that used in Ref 16(CHECK). Varying the broadening around these values does not change the resulting thermal conductivity k_{AF} significantly (see Section).

IV. VIBRATIONAL PROPERTIES

A. Density of States

In this section, we examine the frequencies and density of states (DOS) for the Gamma modes for our models of a-SiO_2 and a-Si. The vibrational DOS is computed by

$$DOS(\omega) = \sum_i \delta(\omega_i - \omega), \tag{13}$$

where a unit step function is used to broaden $\delta(\omega_i - \omega)$.(cite) The DOS for a-$SiO_2$ and a-Si are plotted in Fig. 2 using a broadening of $10\delta\omega_{avg}$ and $100\delta\omega_{avg}$. Because of the finite model size, the low-frequency modes are sparse and the DOS can depend on the broadening.[16] We use a broadening which is large enough to obtain good statistics but also small enough to extend to low frequencies.

The DOS for a-Si is similar to the DOS of crystalline silicon,[59,60] particularly at low-frequency, and with pronounced features at mid-range and high frequencies, as in disordered lattices.[48,61] The DOS for a-SiO_2 is essentially constant over most of the frequency-range, with a gap at the higher frequencies due to the presence of the oxygen atoms.(cite) There is a clear scaling of $DOS \propto \omega^{-2}$ for both a-Si and a-SiO_2 at the lowest frequencies. The onset of this scaling occurs at a higher frequency for a-Si than a-SiO_2. The DOS scaling at the lowest frequencies for a-SiO2 and a-Si suggest that the modes may be propagating (phonon-like), which is investigated in the following sections.

B. Structure Factor

Calculating the structure factors of the supercell Gamma modes is a method to test for their propagating plane-wave character at a particular wave vector and polarization.[16,62]

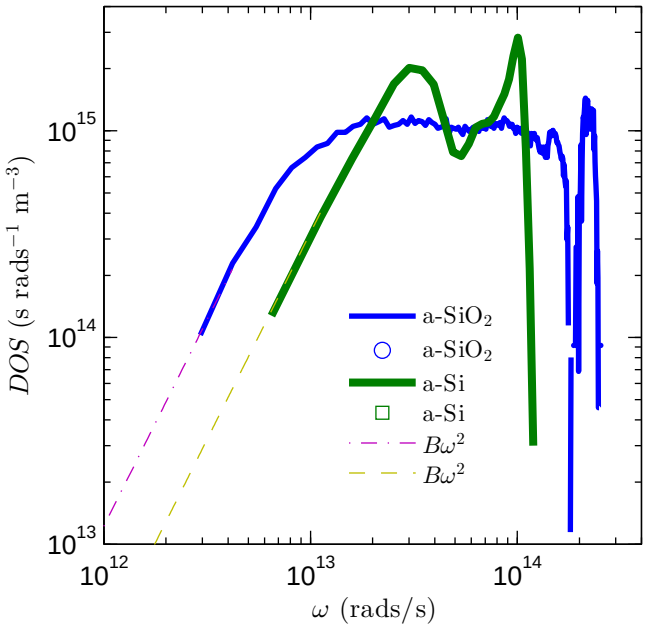

FIG. 2: Vibrational DOS predicted for our models of a-SiO2 and a-Si using Eq. (13). Both models show a scaling at low frequency $DOS(\omega) \propto \omega^{-2}$, which is predicted by the Debye approximation (Eq. (3)) using the transverse sound speeds predicted using various methods (Table I). At high frequency, the DOS of a-SiO2 shows a plateau and then a sharp feature corresponding to a gap in the vibrational spectrum due to the Si and O bonds.(cite) For a-Si, there are two sharp peaks, which show as small peaks in the predictions of the vibrational mode lifetimes (Fig. 4) and mode diffusivities (Fig. 5).

The structure factor has been used to predict effective dispersion of amorphous materials experimentally(cite more)[63] and numerically (cite more).[16,64] The structure factor at a wave vector $\boldsymbol{\kappa}$ is defined as[62]

$$S^{L,T}(\omega^{\boldsymbol{\kappa}}) = \sum_{\nu} E^{L,T}(\nu^{\boldsymbol{\kappa}})\, \delta(\omega - \omega(\nu^{\boldsymbol{\kappa}=\mathbf{0}})), \tag{14}$$

where the summation is over the Gamma modes, E^T refers to the transverse polarization and is defined as

$$E^L(\nu^{\boldsymbol{\kappa}}) = \left| \sum_b \hat{\boldsymbol{\kappa}} \cdot e(\nu^{\boldsymbol{\kappa}=\mathbf{0}}\ {}^{b}_{\alpha}) \exp[i\boldsymbol{\kappa} \cdot \boldsymbol{r}_0({}^{l=0}_{b})] \right|^2 \tag{15}$$

and E^L refers to the longitudinal polarization and is defined as

$$E^T(\nu^{\boldsymbol{\kappa}}) = \left| \sum_b \hat{\boldsymbol{\kappa}} \times e(\nu^{\boldsymbol{\kappa}=\mathbf{0}}\ {}^{b}_{\alpha}) \exp[i\boldsymbol{\kappa} \cdot \boldsymbol{r}_0({}^{l=0}_{b})] \right|^2 . \tag{16}$$

In Eqs. (15) and (16), the b summations are over the atoms in the disordered supercell, $\boldsymbol{r}_0(^{l=0}_{b})$ refers to the equilibrium atomic position of atom b, l labels the unit cells ($l = 0$ for the supercell), α labels the Cartesian coordinates, and $\hat{\boldsymbol{\kappa}}$ is a unit vector. The vibrational "mode shape" is contained in the $3N_a$ components of its eigenvector, $e(^{\boldsymbol{\kappa}=\mathbf{0}\ b}_{\nu\ \alpha})$.

The structure factors $S^{L,T}(^{\boldsymbol{\kappa}}_{\omega})$ are plotted in Fig. 3 for a-SiO_2 and a-Si (left and right panels) for wavevectors along the [100] direction of the supercells. Because of isotropy, the direction is not important and the wavenumber can be considered instead of wavevector. The wavenumbers are normalized by a length scale a so that $\kappa = 1$ corresponds to $2\pi/a$. The length scale $a = 4.8(5.43)$ $\mathring{A}$ for a-SiO_2(a-Si), which is based on the lattice constants of c-SiO2(c-Si).(cite)

Frequencies $\omega_0(\kappa)$ and linewidths $\Gamma(\kappa)$ are predicted by fitting each structure factor peak $S^{L,T}(^{\boldsymbol{\kappa}}_{\omega})$ to a Lorentzian function

$$S^{L,T}(^{\boldsymbol{\kappa}}_{\omega}) = \frac{C_0(\boldsymbol{\kappa})}{[\omega_0(\boldsymbol{\kappa}) - \omega]^2 + \Gamma^2(\boldsymbol{\kappa})}, \tag{17}$$

where $C_0(\nu)$ is a constant related to the DOS.[61] A dispersion relation is identified by plotting $\omega_0(\kappa)$ in the middle panel of Fig.3, where the error bars indicate the linewidths $\Gamma(\kappa)$.

For a-Si, the peaks are reasonably Lorentzian for all wavenumbers considered.[65] For a-SiO2, the peaks are well-approximated as Lorentzian only at the smallest wavenumbers. For large wavenumber, the structure factors peaks are much less than an order of magnitude larger than the background, and the widths are on the order of the frequency range considered in Fig. 3.(cite) For large wavenumber the structrue factor takes on the form of the vibrational DOS.

Fig 4 shows the dispersion extracted by locating the peaks in the structure factor for a-SiO2 and a-Si. For a-Si, the dispersion is nearly linear at small κ with slight concave-down dispersion at high κ.(cite) For a-SiO2, the dispersion is concave-down for the smallest wavenumbers considered, transitioning to a strong concave-up dispersion at intermediate wavenumber. For intermediate κ, the longitudinal dispersion for a-SiO_2 is better-described by the so-called "dispersion law for diffusons", where $\omega \propto \kappa^2$.[61] This large concave-up dispersion has been observed in various amorphous models[65] including of a-SiO2.[66] The dispersion predited by the structure factors show that a-Si has a near-linear, crystal-like dispersion while the dispersion for a-SiO2 is more diffuson-like,(cite) at least over the range of wavenumber and frequencies considered here. At lower frequencies ($<$ 100 GHz)(cite),

experimental measurements of a-SiO2 show a linear dispersion.

C. Group Velocity

The DOS and structure factors predicted in Sections and are now used to predict the group velocity of modes at the lowest-frequencies for a-SiO2 and a-Si. In the low-frequency, long-wavelength limit the mode group velocities are the sound speed.(cite) By fitting the DOS from Fig. 2 to Eq. (3), a sound speed is predicted $v_{s,DOS}$ and reported in Table I. Because the DOS is a mixture of transverse and logitudinal modes only a single sound speed is predicted. Both logitudinal and transverse sound speeds can be predicted from the structure factor.(cite) Sound speeds are estimated from the structure factor peaks by finite differencing,

$$v_s = \frac{\delta\omega_0(\kappa)}{\delta\kappa}, \tag{18}$$

and are shown in Table using the lowest frequency peaks from Fig. 3. The transverse and longitudinal sound speeds of a material can also be predicted from the material's bulk (G) and shear (K) moduli.(cite) The transverse sound speed is given by(cite)

$$v_{s,T} = \frac{G}{\rho}^{1/2}, \tag{19}$$

and the longitudinal by

$$v_{s,L} = \frac{4G + 3K}{3\rho}^{1/2}. \tag{20}$$

We use the bulk and shear moduli defined in terms of the elastic constants according to the Voight convention.(cite) The sound speeds calculated from the elastic constants are reported in Table . The sound speeds predicted for a-Si in Table are in good agreement with those found in a previous study using a similar model.[14,16] Comment about a-SiO2 sound speeds with expt and modeling.(cite)

It is clear that the DOS of our models for a-Si and a-SiO_2 are characterized by using the transverse sound speeds, rather than an averaging of the transverse and longitudinal which is commonly used,(cite)

$$v_s = \frac{2}{3}v_{s,L} + \frac{1}{3}v_{s,T}. \tag{21}$$

The values of the transverse sound speeds obtained from the elastic modulii are somewhat larger than the structure factors, an indication of the concave-down dispersion seen at low

wavenumber, particularly for a-SiO2 (Fig.). (cite) For a-SiO2, the concave-down dispersion also affects the low-frequency DOS, where the predicted sound speed $v_{s,DOS}$ is less than that predicted from the structure factor and the elastic constants (Table). The concave-down dispersion is less pronounced for a-Si, where the sound speeds predicted by all three methods are within five percent of each other.

Under the Debye model (Eq.), the *smaller* transverse sound speed makes the *larger* contribution to the DOS, scaling as the sound speed cubed. For a-Si, the contribution from longitudinal modes to the Debye DOS is nearly an order of magnitude less than the transverse modes for a given frequency interval. For a-SiO_2, the longitudinal and transverse sound speeds are closer, but the concave-down dispersion is stronger than a-Si (Fig.).(cite experimental DOS) The intensity of the structure factors are directly proportional to the DOS.(cite) The intensity for the dynamic structure factor of transverse polarizations has been found to be four to five[67] and 6-8[68] times larger than longitudinal polarizations for models of a-SiO2, which supports our finding that the DOS is dominated by transverse modes. The transverse sound speed predicted by the DOS $v_{s,DOS}$ is used for both a-SiO_2 and a-Si throughout the rest of this work and is discussed in Section .

For a disordered solid, except for the transverse and longitudinal sound speeds, there is not an accepted method to predict the group velocity of each vibrational mode. While the structure factor gives the frequency spectrum needed to construct a propagating state with pure wavevector $\boldsymbol{\kappa}$, the mode spectrum $E^{T,L}(\boldsymbol{\kappa}_\nu)$ (Eqs. and) predicts the plane-wave character of each mode. As shown previously, it is not possible in general to assign a unique wavevector to individual modes, even at low frequency,[14,69,70] which makes predicting individual mode group velocities challenging. Attempts have been made to predict individual mode group velocities,[19,45,50,60,71,72] but it is not clear that these methods are consistent with the predictions made by the structure factor, in this work and in others.(cite) In the Cahill-Pohl (CP) model, for example, the group velocity of all disordered modes is the sound speed, v_s, which is also assumed for the HS model Eq. (**??**).[45] This assumption is not generally valid for any material.[16,19,48,50,60,71] To treat this problem, the thermal diffusivities of vibrational modes in a-SiO2 and a-Si are predicted and compared in Section to test the assumption of the mode group velocities at all frequencies.

TABLE I: Estimated from the elastic constants, the pre-annealed group velocities are $v_{s,T,} = 3,670$, $v_{s,L,elas} = 7,840$ for a-Si and $v_{s,T,elas} = 2,541$, $v_{s,L,elas} = 4,761$ for a-SiO2 (see Section IV C).

method	Eqs. (19), (20)	Eqs. (14), (18)	DOS Eq. (3)
a-SiO_2			
transverse	3,161	2,732	2,528
longitudinal	5,100	4,779	
a-Si			
transverse	3,886	3,699	3,615
longitudinal	8,271	8,047	

D. Mode Lifetimes

We now predict the lifetimes of all vibrational modes in our models of a-SiO2 and a-Si using the MD simulation-based normal mode decomposition (NMD) method.[73–76] The NMD-predicted lifetimes will be compared with the timescales extracted from the structure factor linewidths, $\tau_{SF} = 1/2\Gamma(\kappa)$ (Section , (Eq. (17))). The NMD method can predict vibrational lifetimes which are affected by the disorder in the supercell.[19,48,50,77**?**]

In NMD, the atomic trajectories from MD simulations are first mapped onto the vibrational mode coordinate time derivative,[37]

$$\dot{q}(\substack{\boldsymbol{\kappa}=\mathbf{0} \\ \nu}; t) = \sum_{\alpha,b,l}^{3,n,N} \sqrt{\frac{m_b}{N}} \dot{u}_\alpha(\substack{l \\ b}; t)\, e^*(\substack{\boldsymbol{\kappa}=\mathbf{0} \\ \nu} \substack{b \\ \alpha}) \exp[i(\mathbf{0} \cdot \mathbf{r}_0(\substack{l \\ 0})]. \tag{22}$$

Here, m_b is the mass of the b_{th} atom in the supercell, u_α is the α-component of the atomic displacement from equilibrium, $\dot{u}_\alpha$ is the α-component of the atomic velocity, and t is time. Because the supecells of a-SiO2 and a-Si are disordered, the NMD method is performed at the wavevector $\boldsymbol{\kappa} = \mathbf{0}$. The spectral energy of each vibrational mode, $\Phi(\substack{\boldsymbol{\kappa} \\ \nu}; t)$, is calculated from

$$\Phi(\nu, \omega) = \lim_{\tau_0 \to \infty} \frac{1}{2\tau_0} \left| \frac{1}{\sqrt{2\pi}} \int_0^{\tau_0} \dot{q}(\substack{\boldsymbol{\kappa}=\mathbf{0} \\ \nu}; t) \exp(-i\omega t) dt \right|^2. \tag{23}$$

We choose the frequency domain representation of the normal mode energy because it is less sensitive to any meta-stability of the amorphous structure.(footnote) (footnote)In an amorphous material, there are many potential energy configurations (atomic positions) which are nearly equivalent in energy. At a sufficient temperature, the meta-stable configurations cause the equilibrium atomic positions to vary in time. This can effect on the prediction

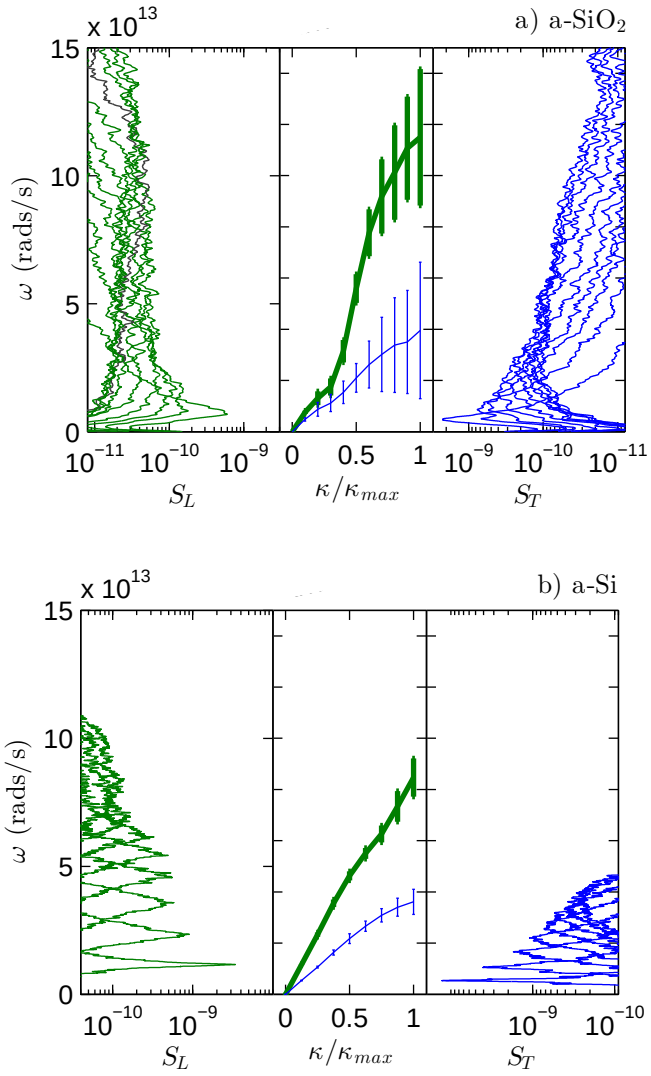

FIG. 3: Longitudinal (left panel) and transverse (right panel) structure factors (Eq. (14)) for a-SiO2 (top plot) and a-Si (bottom plot). Sound speeds are estimated by finite differencing (Eq. (18)) of the lowest frequency peaks and are reported in Table I. The dispersion for a-SiO2 is only linear for the lowest frequency, smallest wavenumbers. The dispersion for a-Si is linear over a wider range of wavenumber. Lifetimes are predicted from the widths of the structure factor peaks (Eq. (17)) and are plotted in Fig. 4.

of the vibrational mode lifetimes when using the normal mode decomposition method. In the time domain, the average normal mode potential and kinetic energy must be calculated and subtracted from the normal mode energy autocorrelation function.(cite) If the average energy is not specified correctly, unphysically large or small mode lifetimes can be predicted.(cite)

The vibrational mode frequency and lifetime is predicted by fitting each mode's spectral energy $\Phi(\nu, \omega)$ to a Lorentzian function

$$\Phi(\nu, \omega) = \frac{C_0(\nu)}{[\omega_0(\nu) - \omega]^2 + \Gamma^2(\nu)}, \tag{24}$$

where the constant $C_0(\nu)$ is related to the average energy of each mode and the linewidth $\Gamma(\nu)$ and is valid when $\Gamma(\nu) < \omega_0(\nu)$.[76] The mode lifetime is given by(cite)

$$\tau(\nu) = \frac{1}{2\Gamma(\nu)} \tag{25}$$

The NMD-predicted lifetimes are plotted in Fig. 4 for a-SiO2 and a-Si. For a-SiO2, the mode lifetimes are generally larger than the IR limit $\tau = 2\pi/\omega$,(cite) and follow this limit at low frequency. There is no clear evidence for a quadratic scaling $\tau \propto \omega^{-2}$, which corresponds to a quadratic scaling of the diffusivity at low frequency where the group velocity is constant (Eq. (4)). At high frequency the mode lifetimes are roughly constant without definite scaling. There is a peak near 2 10^{14} rads/s which corresponds to a peak in the DOS (see Fig. 2). The lifetimes predicted from the structure factor fall below the NMD-predicted lifetimes and the IR limit. This is because the structure factor for a-SiO2 is evaluated for large enough wavenumber that the peaks are not well-approximated as Lorentzian.(cite) Fitting the peaks we find the linewidth (inverse lifetime) to be on the order of the frequency range considered in Fig. 3. Models(cite) and theoretical(cite) predictions show that the structure factor begins to take on the form of the DOS for large enough wavenumber,[24,78] and the linewidths (timescales) are not meaningful. For a-SiO2 the NMD and structure factor-predicted lifetimes indicate that the low-frequency modes in our model are not well-characterized as propagating.(cite)

For a-Si, The mode lifetimes show a clear scaling at low frequency $\tau \propto \omega^{-2}$. The lifetimes plateau at higher frequencies, over a wider range of frequencies than a-SiO2, with two peaks corresponding to peaks in the DOS (Fig. 2). The plateau of lifetimes at high frequencies has been reported for disordered lattices[48,79] and other models of a-Si.[50] The transition

from the quadratic low-frequency scaling to the plateau region occurs near 10^{14} rads/s, which corresponds to where the DOS peaks in Fig. 2. Similar behavior was observed for models of disordered lattices.[48] The lifetimes predicted by the structure factor are in good agreement with those predicted by NMD at low frequencies. Similar agreement has been reported in other models of topologically disordered materials.[80] The longitudinal and transverse polarizations outline the scatter in the NMD-predicted lifetimes. While the DOS at low frequency is dominated by transverse modes, the NMD and structure factor-predicted lifetimes indicate there is some mixture of longitudinal and transverse-like modes.(cite)

The NMD-predicted lifetimes in this work are similar in magnitude to those predicted for previous models of a-Si.[81,82] Fabian and Allen find lifetimes on the order of picoseconds for a-Si[83] and para-crystalline silicon.[84] A previous study of Tersoff a-Si predicted vibrational lifetimes on the order of 100 ps, about ten times the values reported here and in other studies.(cite) It is unclear what the source of this discrepancy is, although the analysis in Ref 19 the NMD method in the time domain. Using the Tersoff potential on the WWW a-Si models in this work we find... Predicted lifetimes are also similar for samples created using a melt-quench technique (see Section **??**).

E. Diffusivities

Using the sound speeds predicted from the DOS $v_{s,DOS}$ (Table), the NMD-predicted lifetimes are used to predict the mode diffusivities with Eq. (4) and are shown in Fig. for a-SiO2 and a-Si. The sound speed is most appropriate for the lowest-frequecy modes (see Section). To compare with the NMD predictions, the AF theory is also used to predict the mode diffusivities (see Section) which are shown in Fig. .

For a-SiO2 at the lowest frequencies, the diffusivities scale roughly as Eq. with $n = 2$. However this scaling is not definitive for the diffusvities predicted by either method, particularly for the NMD predictions, which is apparent from the scaling of the NMD-predicted lifetimes in Fig. . To identify the transition from propagating to non-propagating modes, we use $\omega_{cut} = 4.55$ rad/s for Eq. , the same as that used in Ref 24 since there is no clear indication of this tranistion from Fig. . This choice is discussed in Section . The constant $B =$ is Eq. is fit to the AF-predicted diffusivities for $\omega \leq \omega_{cut}$.

For a-Si at low frequencies there is a clear scaling of the diffusivities Eq. with $n = 2$. The

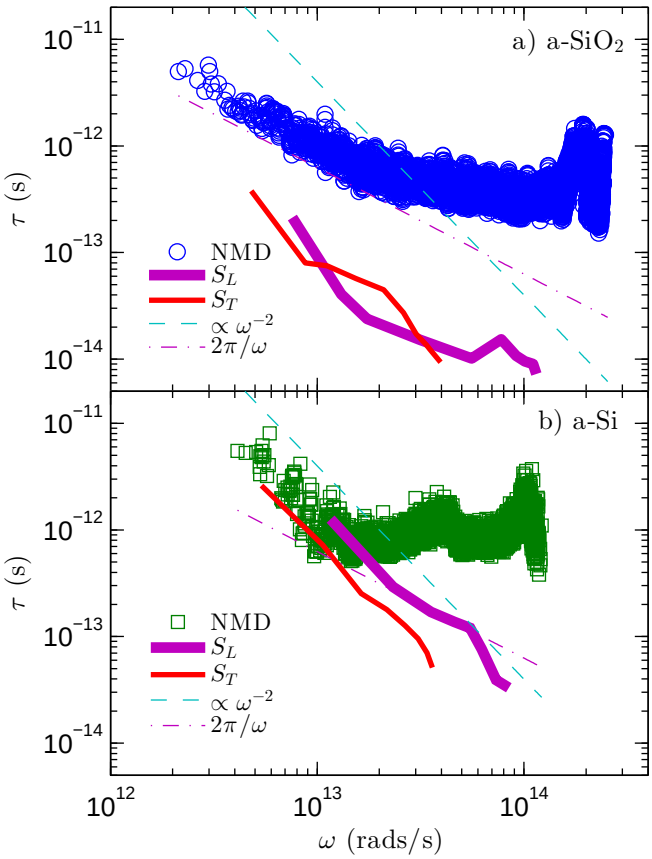

FIG. 4: vibrational mode lifetimes predicted by NMD (Eq. (25)) and the structure factors (Eq. (17)) for a-SiO2 (top plot) and a-Si (bottom plot). The IR limit is a lower limit for the NMD-predicted lifetimes, while the lifetimes from the structure factors fall below this limit, particularly for a-SiO2. The structure factor lifetimes generally follow a scaling $\tau \propto \omega^{-2}$ for both systems, while the NMD-predicted lifetimes show a plateau before crossing the IR limit.

NMD-predicted diffusivities show much less scatter than those predicted by the AF theory, which is due to the finite-size system and the broadening which is required to evaluate Eq. (10).[14] By using a much larger broadening ($100\delta\omega_{avg}$) the scatter in the AF-predicted diffusivities at low frequency can be smoothed, but at the cost of decreasing the diffusivities at intermediate and high frequencies. It is possible that a frequency-dependent broadening may be necessary for a-Si and the AF theory,(cite) but determining this dependence is not clear nor necessary for interpreting the results in this work.

For a-Si, we choose ω_{cut} and B so that Eq. is equal to the AF-predicted diffusivity at $\omega = \omega_{cut}$. This choice allows Eq. to pass reasonably well through both the AF and NMD-

predicted diffusivities. The value of ω_{cut} and B are comparable to those used in Ref. . For a-Si we also consider a separate scaling for Eq. with $n = 4$ which is discussed in Section . Because this scaling is not clear from the data in Fig. we use $\omega_{cut} = 1.52\ 10^{1}3$ rads/s from Refs. **??** and **??** and choose B so that Eq. is equal to the AF-predicted diffusivity at ω_{cut}. We discuss these choices in Section .

For a-SiO2, the mode diffusivities predicted by NMD and AF agree well over the entire frequency range. At high frequencies the diffusivities do not vary much, except for a peak for the NMD predictions near $2\ 10^{14}$ rads/s which corresponds to the same peak in lifetimes (Fig.). For the AF predictions, the mode diffusivities near $2\ 10^{14}$ rads/s and at the highest frequencies show a sharp decrease, which is an indication that these modes are localized.(cite)

Both a-SiO_2 and a-Si have a region at higher frequencies where the AF-predicted mode diffusivities are relatively constant. This behavior has been reported for a number of model disordered systems such as disordered lattices[48,61,79], amorphous solids,[19] and jammed systems.[85,86] For a-Si the NMD- and AF-predicted diffusivities diverge near $1\ 10^{13}$ rads/s, while the NMD-predicted lifetimes are relatively constant above this frequency. This implies that the velocity scale for diffusons,

$$v_{AF}(\omega) = \left(3\frac{D_{AF,i}(\omega)}{\tau(\omega)}\right)^{1/2}, \tag{26}$$

is a function of frequency. At low frequencies, v_{AF} reaches as high as $v_{s,DOS}$ and decreases to about $(1/3)v_{s,DOS}$ at higher frequencies. This variation of $v_{AF}(\omega)$ is similar to the variation of the group velocity which can be estimated from the dispersion relation found in Fig. . For a-SiO2, v_{AF} is near $v_{s,DOS}$ over the whole frequency range, which is the assumption made for the high-scatter limit Eq. .

(WORK)

The dependence of v_{AF} with frequency for a-Si is similar to that found for simple crystalline systems, where negative dispersion typically causes a decrease of group velocity with increasing frequency (or wavevector).(cite) Negative dispersion has been predicted by many models of both a-SiO2 and a-Si,[87] as have experimental measurement of dispersion relations.(cite) The effective group velocities which have been predicted using dispersion relations near zero wavevector for large supercells of amorphous[19,50] and disordered lattices[72] would appear to be underestimates compared with the effective velocities v_{AF} predicted in this work, where v_{AF} is within a factor of three of v_s for all but the highest frequency, lo-

calized modes.(cite) Our predictions for v_{AF} also support the notion of a minimum thermal diffusivity on the order of D_{HS} for all vibrational modes except those which are localized (the so-called "locons").(cite)

While diffusons are non-propagating modes whose MFPs are not well-defined, a diffuson MFP can be defined as

$$\Lambda_{AF}(\omega) = (3D_{AF,i}(\omega)\tau(\omega))^{1/2}, \tag{27}$$

where $\tau(\omega)$ are the NMD-predicted lifetimes. Using this definition, $\Lambda_{AF}(\omega)$ is found to vary for a-SiO2 and a-Si between the supercell size L and the lattice constant a (see Section) for modes with $\omega > \omega_{cut}$. Similar MFPs have been estimated for a-Si in previous studies.[14,16] This is in contrast to the MFPs estimated in Ref 50 which were found to be up to approximately $70L$. The reason for this discrepancy is some combination of the predicted lifetimes and the method with which the mode group velocities were estimated.[50]

V. THERMAL CONDUCTIVITY

A. Bulk

To predict the bulk thermal conductivity for our models of a-SiO2 and a-Si, we use Eq. (1) and the GK method.(cite) The GK method for predicting thermal conductivity is relatively inexpensive compared to the NMD and AF methods so large system sizes can be studied (see Section **??**). Similarly-large systems were studied in Ref. 50. The details of the GK method are discussed in Section III B.

The GK-predicted thermal conductivity k_{GK} is plotted in Fig. 6 for varying system sizes L. For a-SiO2, there is no apparent dependence of k_{GK} on L and $k_{GK} = 2.1 \pm 0.15$ W/m-K. For a-Si, there is a clear dependence of k_{GK} on L. Assuming the DOS has the form of Eq. (3) and the diffusivity scaling is Eq. (7) with $n = 2$ for the low-frequency modes in the system, the thermal conductivity as a function of the system size takes the form

$$\frac{k(L)}{k_{bulk}} = 1 - \frac{c_0}{L}, \tag{28}$$

where k_{bulk} is the extrapolated bulk thermal conductivity and c_0 is a constant.[88,89] The extrapolation is performed using the three largest system sizes studied, including the tiled

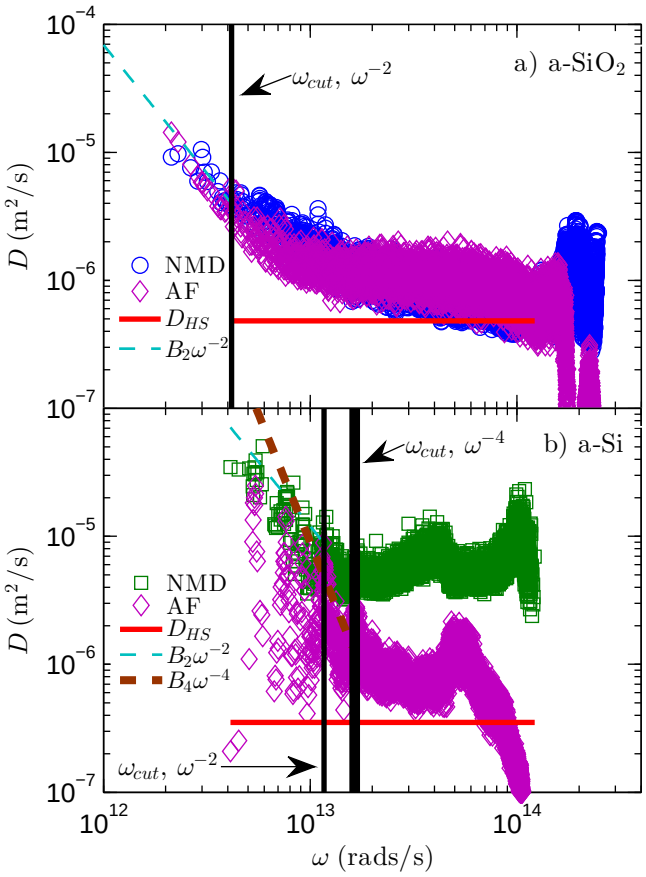

FIG. 5: vibrational mode diffusivities predicted from NMD (using Eqs. (4) and (25) with the sound speed $v_{s,DOS}$ from Table I) and AF theory (Eq. (10)). Also shown are the extrapolations Eqs. (7) and (**??**), which are used with Eq. (2) to predict the thermal conductivity accumulations in Fig. 8, and the high-scatter limit Eq. (11).

800,000 atom sample (see Section **??**). We do not observe that tiling an a-Si model increases the thermal conductivity of a given system size above that predicted by Eq. , as was found in Ref 19 using the MD-based direct method. This is likely due to the small (512 atom) model used to perform the tiling in that study, while we use a 100,000 atom model. The success of Eq. (28) for the dependence of k_{GK} on L for our model of a-Si is in agreement with the scaling Eq. (7) with $n = 2$ (Fig. 5 and the Debye-scaling of the DOS (Fig. 2). The extrapolated $k_{bulk} = 1.9 \pm 0.1$ W/m-K

To predict k_{vib} (Eq.) we use the input parameters B, ω_{cut}, and the AF-predicted diffusivities $D_{AF}(\omega)$ obtained in Section . For a-SiO2, $k_{AF} = 1.92$ and $k_{pr} = 0.09$ W/m-K.

Baldi et al find that the contribution k_{ph} 0.1 W/m-K, which is the same as the contribution k_{ph} predicted in this work for a-SiO2. This contribution k_{ph} is smaller than the error bars in the predictions of k_{vib} and k_{GK} shown in Figs. and .

For a-Si with Eq. and $n = 2$, $k_{AF} = 1.16$ and $k_{pr} = 0.62$ W/m-K. For Eq. and $n = 4$, the diverging conductivity at low frequency is fixed by the use of a simple boundary scattering model based on the Matthiesen rule and the thin-film thickness t_f,[90]

$$\frac{1}{\Lambda_{eff}} = \frac{1}{\Lambda_{bulk}} + \frac{2}{t_f}. \tag{29}$$

Using

$k_{pr} = 2.98$ W/m-K

Using the $n = 2$ scaling and $t_f = 80,000$ nm does not change k_{pr} within the precision reported. For $t_f = 50$ nm, $k_{pr} = 0.22$ for $n = 4$ and $k_{pr} = 0.34$ for $n = 2$.

We predict for a-Si $k_{ph} = 0.62$ W/m-K. Similar values for k_{ph} can be predicted by increasing ω_{cut} and decreasing B.

The same ω_{cut} was used by Cahill et al. together with a Rayleigh scaling and a boundary scattering model to find $k_{ph} = 0.31$ W/m-K.[15]

Comparing with previous MD simulations of a-Si, Lee found a value of around 1 W/m-K but with very small supercell sizes.[91] He et al find for bulk a-Si $k_{vib} = 3$ W/m-K using the Tersoff potential and a linear extrapolation of the form Eq. using non-equillibrium molecular dynamics. In this study He at al find that $k_{pr} \approx k_{AF} \approx 1.5$ W/m-K. Regner et al find a plateau in k_{vib} for large broadband FDTR frequencies implying that $k_{AF} \approx 1$ W/m-K.(cite)

Assuming a constant contribution $k_{AF} \approx 1$ W/m-K, experimental measurements and estimates show that the contribution from k_{pr} is 20%,

While the classic limit for the mode specific heat is an over-prediction for the high frequency modes in a-Si, the non-propagating contribution predicted by broadband FTDR matches the prediction from the AF diffuson theory. Adjusting the specific heats to include quantum statistical effects...

We can thus focus on the less understood low-frequency propagating contribution.

For a diffusivity scaling Eq. with $n = 4$ the thermal conductivity is divergent in the zero frequency limit. The s

Phonon-like behavior can be identified for a-Si in this work and others, both experimentally[12,17,18,20] and numerically.[14,16,50,51] Including the phonon-like contribution k_{ph}

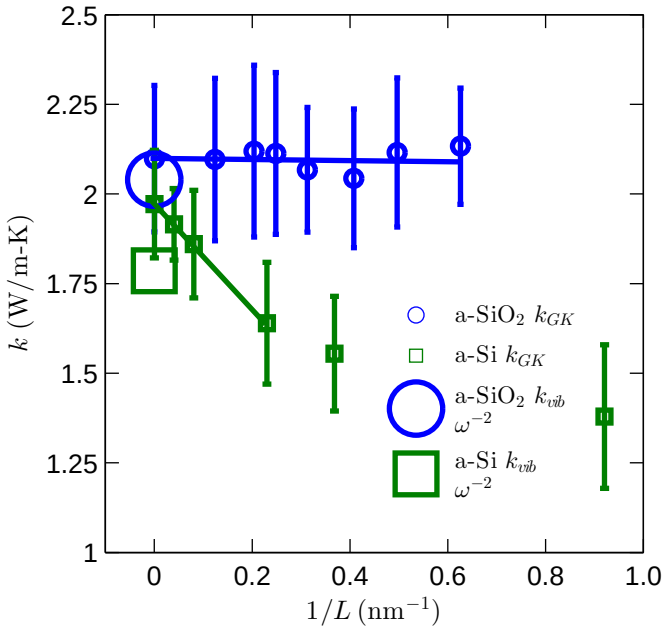

FIG. 6: Thermal conductivities of a-SiO_2 and a-Si prediced using the GK method. For a-SiO2, the thermal conductivity is size-independent, indicating there is no important contribution from phonons (Eq. (2)). For a-Si, there is a clear size dependance, which is accounted for by using Eq. (2) and an ω^{-2} extrapolation (Eq. (7), Fig. 5).

for a-Si is not qualitatively sensitive to the choice of model[14,16,17] or ω_{cut}.[14,16–18,60]

B. Accumulation Function

BEGINALAN

The thermal conductivity accumulation function,

$$k(\Lambda_{cut}) = \frac{1}{V}\int_0^{\Lambda_{cut}} kbD(\Lambda)DOS(\Lambda) + \frac{1}{V}\sum_{\Lambda<\Lambda_{cut}} kbv_{AF}\Lambda_{AF}, \tag{30}$$

is predicted using our models of bulk a-SiO2 and a-Si and shown in Fig. . For the phonon contribution k_{ph}, the mode diffusivities ($D(\omega)$ can be transformed $D(\Lambda) = D(\omega)/v_s$.

The thermal conductivity accumulation functions for a-SiO2 and a-Si thin films are shown in Fig. . The thermal conductivity accumulation function for a-SiO2 saturates at a MFP of 10 nm, which is on the order of the finite size of our model (Section III A). This sharp accumulation at small MFPs is in good agreement with the prediction that k_{AF} is the dominant

contribution to k_{vib}. This result is also in accord with the penetration depth-independent thermal conductivity measurements using broadband FDTR.[20] Only the quadratic scaling is considered for a-SiO2, which is discussed later in Section V B.

For a-Si, the thermal conductivity accumulation function shows that k_{AF} saturates before 10 nm, which is also on the order of our finite model size. The propagating contribution k_{ph} is predicted using both quadratic and quartic scaling for the mode diffusivities. As discussed in Section V, the quadratic scaling is responsible for the system size dependent thermal conductivity predicted by the GK method (k_{GK}, see Section V) and seems to be the correct scaling to describe the low-frequency modes for our model of bulk a-Si. Using the quadratic scaling, the thermal accumulation functions for our model of a-Si thin films passes reasonably well through many of the experimentally measured values.(cite) The quartic scaling also passes through many of the experimentally measured values reasonably well, particularly for film thicknesses larger than 10 μm.(cite)

ENDALAN

C. Discussion

BEGINALAN

Previous experimental studies of a-SiO2 have estimated negligible the contribution from low frequency ($\omega < \pi 10^1 2 rads/s$)[92] vibrational modes to be negligible. Using our model of a-SiO2, we also find the low-frequency propagating contribution to be negligible (Section V B). While experiments show there is are cross-over regions from quadratic to quartic scaling of the mode lifetimes in a-SiO2, the thermal conductivity of thin film a-SiO2 shows no significant dependence on the thickness.(cite) The cross-over region from quadratic to quartic, then back to quadratic observed in experiments for a-SiO2 occurs in the frequency range 4.610^9 to 1.5210^{10} rads/s,[23] and $3.0410^1 1$ to 1.5210^{12} rads/s[27]. While these frequency ranges are inaccessible by our finite- size models, we estimate that the extrapolated k_{ph} using a quartic scaling in this region to be...

The transverse sound speed predicted for our model of a-SiO2 is about 85% of that measured by experiment.[17] While using a smaller transverse sound speed leads to an underprediction of the mode diffusivity scalings (Eq. (4), Fig. 5), it leads to an overprediction of the DOS (Eq. (3)). Overall this leads to an underprediction of the thermal conductivity

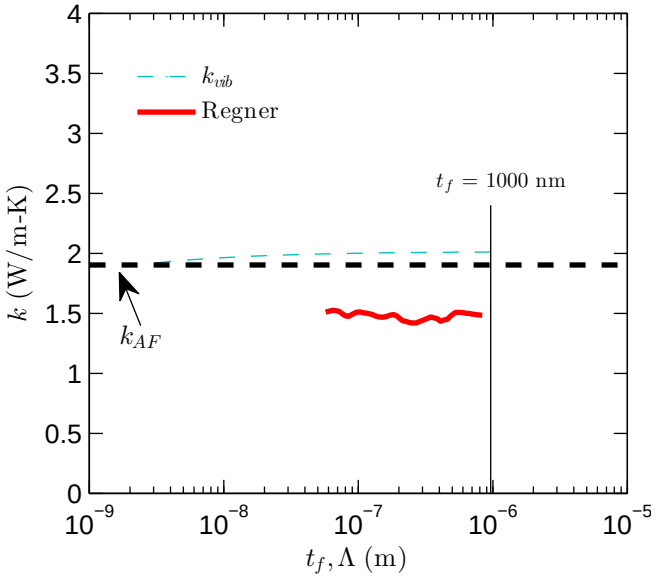

FIG. 7: Thermal conductivity accumulations and thermal conductivities versus film thickness for a-SiO2 (top plot) and a-Si (bottom plot) from: (i) predictions from this work, (ii) recent broadband measurements of Regner et al, (iii) various experimental measurements for a wide-range of a-Si film thicknesses. While the thermal conductivity predictions for a-SiO2 and a-Si in this work seem to be well-characterized by Umklapp type scaling of the MFPs (Eq. (7)), this scaling is not able to predict the dramatic increase of thermal conductivity with increasing film thickness from experimental measurements of a-Si thin films.

because the DOS scales as $DOS(\omega) \propto 1/v_s^3$. We can regard the predictions from our models, with smaller transverse sound speeds, as an upper bound on k_{ph} for a given diffusivity scaling $D(\omega) = B\omega^{-2}$. The critical parameter is the choice of ω_{cut}.(cite) We pick ω_{cut} and the low frequency scaling $D(\omega) = B\omega^{-2}$ based on their ability to describe the low-frequency behavior of the vibrational modes in our finite-size models. The quadratic scaling $D(\omega) = B\omega^{-2}$ has been observed in separate numerical studies for models of a-SiO2(cite) and a-Si(cite).

The bulk thermal conductivity predicted for our model of a-SiO2 overestimates that of experimental measurements.[20] This can be attributed to either difference between experimental a-SiO2 and the potential model used in this work,(cite) the lack of anharmonic scattering included in the AF theory,[14] or the assumption of the classical-limit specific heat for all frequencies (Section II). Qualitatively, our model confirms that propagating modes do not contribute significantly to the thermal conductivity of a-SiO2.

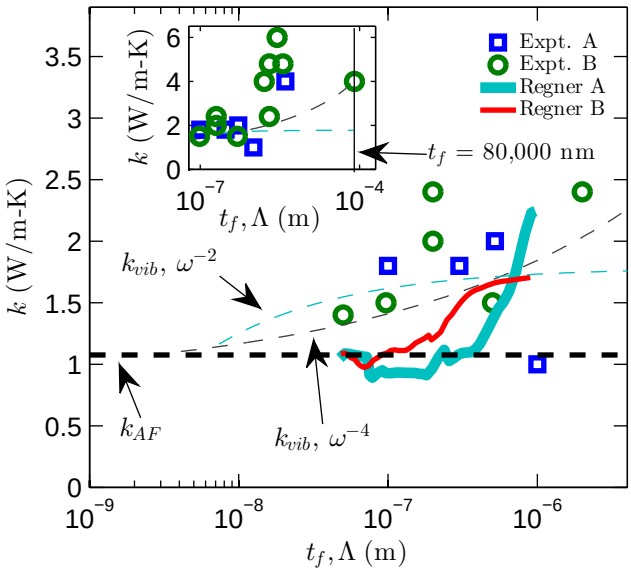

FIG. 8: film thickness dependant thermal conductivity of a-Si from experiment.

The classical-limit mode specific heat is a good approximation for the low-frequency propagating modes in a-SiO2 and a-Si, which are shown to fully activated by around 10 K.(cite) The classic limit for the mode specific heat is an over-prediction for the high frequency modes in a-SiO2 and a-Si at 300 K.(cite) However, the contribution k_{AF} we predict in the classical limit for mode specific heat for a-Si is nearly the same as the the non-propagating contribution (plateau) predicted by broadband FTDR.(cite) Adjusting the specific heats to include quantum statistical effects... Taking the diffuson contribution k_{AF} to be a constant, which we predict to be $k_{AF} \approx 1$ W/m-K in agreement with other numerical studies(cite) and experiments(cite), we can thus focus on determining the less understood low-frequency propagating contribution k_{ph}.

The scaling of the low-frequency lifetimes in a-Si is not clear from the experimental measurement. For a-Si thin films, varying preparation techniques suggest either quadratic(cite) or quartic(cite) scaling. While there is no clear consensus from various experiments, all predictions in this work demonstrate that the low-frequency modes in bulk a-Si follow a quadratic scaling of the mode lifetimes, which has been observed in previous models of a-Si(cite) and a-SiO2.(cite) Amorphous silicon, however, can be prepared only in thin films,(cite) where voids and other inhomogeneities are unavoidable[93] and can influence the vibrational structure at low frequencies.[17,94] A smooth transition between quadratic and

quartic scaling can be achieved using a phenomenological model where a cross-over wavevector (or frequency) must be specified by experiment.[26] While this cross-over can be identified experimentally for a-SiO2,[23] experiments are limited for a-Si thin films.(cite) Our models are not large enough to investigate the relevant frequency range ($< 110^{12}$ rads/s),(cite) so we considered both quadratic and quartic lifetime scalings when predicting the thermal conductivity accumulation functions in Fig. . Experimental measurements of the cross-over frequency (wavevector) and steepness parameter are needed from experiment to investigate the applicability of this phenomenological model further.(cite) The dependence of a-Si thin film thermal conductivity on thickness,(cite) preparation method,(cite) and hydrogen content(cite) make this particularly challenging. In fact, different experimental studies can be satisfactorily explained using quadratic(cite) or quartic(cite) scalings found that each was a satisfactory explanation for the results found. (cite)

A number of emerging experimental techniques are capable of studying the low-frequency propagating modes in disordered systems. (cite) For amorphous materials, where the propagating contribution k_{ph} is typically smaller than in the crystalline phase, broadband FDTR has demonstrated it can probe the relatively small effect of propagating modes at 300 K. However, the broadband FDTR studies thus far have been limited to one deposition technique and a relatively small range of film thicknesses (500 nm $< t_f <$ 2000 nm).(cite) The nature of the low frequency scaling can be better elucidated using broadband FDTR on films prepared using varying deposition techniques,(cite) a wider-range of film thicknesses (1-100 μm) (cite) and lower-range of temperatures ($10 - 100$ K).(cite) For a-Si, propagating low-frequency have been identified qualitatively by both experimental measurements(cite) and numerical modeling.(cite) It is thus interesting to consider thin films of a-SiGe alloys, which have been demonstrated to have reduced thermal conductivities compared to a-Si.[14] It is not clear what vibrational lifetime scaling at low frequency would be observed in a simple topologically disordered alloy given there is no a consensus for even topologically disordered but chemically ordered systems.(cite) A combination of frequency-domain, time-domain, and variable-physical-heating size measurements would be helpful in investigating.[10,12,20,95]

ENDALAN

This supports the idea of Slack for a-SiO_2[96] While the thermal conductivity of a-SiO , the material is characterized by a constant similar for other amorphous materials such as Lennard-Jones argon[48] and a model of a-GeTe.[49]

That the amorphous phase of Si should have a lower GHz attenuation than many other amorphous materials is not entirely surprising, as the 2002 review of low-temperature thermal conductivity and internal friction by Pohl, Liu, and Thompson certainly indicates that the fourfold coordinated materials tend to demonstrate weaker anharmonicity.[97]

Theoretical predictions of acoustic attenuation in amor- phous solids generally agree that at room temperature, a quadratic frequency dependence is expected in the frequency range of 10 GHz1 THz and its origins are expected to be the anharmonicity of the interatomic bonds.

Theory from Schirmacher et al. predicted an w4 scaling below a system dependent onset frequency.[98,99]

VI. SUMMARY

BEGINALAN

In this work we investigated the contributions of propagating k_{ph} and non-propagating k_{AF} modes to the total vibrational thermal conductivity k_{vib} of two glasses, a-SiO2 and a-Si. For a-SiO2, the contribution from propagating modes k_{ph} is shown to be negligible compared to k_{vib}. This is confirmed by various experimental measurements, including a broadband FDTR study which probed the vibrational MFPs or a-SiO2. The thermal conductivity accumulation function for our model of a-SiO2 saturates near a MFP of 10 nm, in agreement with the results of Regner et al. who show no systematic variation of the thermal conductivity on L_p,[20] and in agreement with experiments on a-SiO2 thin films which show no systematic variation with film thickness t_f.(cite)

Our model of bulk a-Si has a thermal conductivity k_{vib} with significant contribution from k_{ph}, where the low-frequency propagating modes are best described by a quadratic scaling of the mode lifetimes. The thermal conductivity accumulation predicted for our model of bulk a-Si with a simple boundary scattering model show reasonable agreement with some of the experimentally predicted thermal conductivities using varying film thicknesses and deposition techniques (Fig.).(cite) However, using a quartic scaling with our model also gives a satisfactory agreement with other experimental measurements (Fig.).(cite) These large discrepancies between measured thermal conductivity of various a-Si thin films calls for the need of further experimentation. Broadband techniques,(cite) which have demonstrated

the ability to probe a wide-range of vibrational mode frequencies and MFPs, can help elucidate.(cite)

ENDALAN

[1] D. G. Cahill, W. K. Ford, K. E. Goodson, G. D. Mahan, A. Majumdar, H. J. Maris, R. Merlin, and S. R. Phillpot, Journal of Applied Physics **93**, 793818 (2003).

[2] J.-K. Yu, S. Mitrovic, D. Tham, J. Varghese, and J. R. Heath, Nature Nanotechnology **5**, 718721 (2010).

[3] A. I. Hochbaum, R. Chen, R. D. Delgado, W. Liang, E. C. Garnett, M. Najarian, A. Majumdar, and P. Yang, Nature **451**, 163167 (2008).

[4] G. Pernot, M. Stoffel, I. Savic, F. Pezzoli, P. Chen, G. Savelli, A. Jacquot, J. Schumann, U. Denker, I. Mnch, et al., Nat Mater **9**, 491 (2010), ISSN 1476-1122, URL http://dx.doi.org/10.1038/nmat2752.

[5] A. I. Boukai, Y. Bunimovich, J. Tahi-Kheli, J.-K. Yu, W. A. G. Goddard, and J. R. Heath, Nature **451**, 168171 (2008).

[6] B. Poudel, Q. Hao, Y. Ma, Y. Lan, A. Minnich, B. Yu, X. Yan, D. Wang, A. Muto, D. Vashaee, et al., Science **320**, 634638 (2008), URL http://www.sciencemag.org/content/320/5876/634.abstract.

[7] A. Ward and D. A. Broido, Phys. Rev. B **81**, 085205 (2010), URL http://link.aps.org/doi/10.1103/PhysRevB.81.085205.

[8] M. G. Holland, Physical Review **132**, 2461 (1963).

[9] A. D. Christianson, M. D. Lumsden, O. Delaire, M. B. Stone, D. L. Abernathy, M. A. McGuire, A. S. Sefat, R. Jin, B. C. Sales, D. Mandrus, et al., Phys. Rev. Lett. **101**, 157004 (2008), URL http://link.aps.org/doi/10.1103/PhysRevLett.101.157004.

[10] Y. K. Koh and D. G. Cahill, Phys. Rev. B **76**, 075207 (2007), URL http://link.aps.org/doi/10.1103/PhysRevB.76.075207.

[11] M. Highland, B. C. Gundrum, Y. K. Koh, R. S. Averback, D. G. Cahill, V. C. Elarde, J. J. Coleman, D. A. Walko, and E. C. Landahl, Phys. Rev. B **76**, 075337 (2007), URL http://link.aps.org/doi/10.1103/PhysRevB.76.075337.

[12] A. J. Minnich, J. A. Johnson, A. J. Schmidt, K. Esfarjani, M. S. Dresselhaus, K. A. Nelson, and G. Chen, Phys. Rev. Lett. **107**, 095901 (2011), URL http://link.aps.org/doi/10.1103/PhysRevLett.107.095901.

[13] F. Yang and C. Dames, Physical Review B **87**, 035437 (2013), URL http://link.aps.org/

doi/10.1103/PhysRevB.87.035437.

[14] J. L. Feldman, M. D. Kluge, P. B. Allen, and F. Wooten, Physical Review B **48**, 1258912602 (1993).

[15] D. G. Cahill, M. Katiyar, and J. R. Abelson, Physical Review B **50**, 60776081 (1994).

[16] J. L. Feldman, P. B. Allen, and S. R. Bickham, Phys. Rev. B **59**, 35513559 (1999), URL http://link.aps.org/doi/10.1103/PhysRevB.59.3551.

[17] X. Liu, J. L. Feldman, D. G. Cahill, R. S. Crandall, N. Bernstein, D. M. Photiadis, M. J. Mehl, and D. A. Papaconstantopoulos, Phys. Rev. Lett. **102**, 035901 (2009), URL http://link.aps.org/doi/10.1103/PhysRevLett.102.035901.

[18] H.-S. Yang, D. G. Cahill, X. Liu, J. L. Feldman, R. S. Crandall, B. A. Sperling, and J. R. Abelson, Phys. Rev. B **81**, 104203 (2010), URL http://link.aps.org/doi/10.1103/PhysRevB.81.104203.

[19] Y. He, D. Donadio, J.-H. Lee, J. C. Grossman, and G. Galli, ACS Nano **5**, 1839\textbackslashtextbackslashtextbackslashtextbackslashtextbackslash961844 (2011).

[20] K. T. Regner, D. P. Sellan, Z. Su, C. H. Amon, A. J. McGaughey, and J. A. Malen, Nat Commun **4**, 1640 (2013), URL http://dx.doi.org/10.1038/ncomms2630.

[21] S.-M. Lee and D. G. Cahill, Journal of Applied Physics **81**, 25902595 (1997).

[22] T. Yamane, N. Nagai, S.-i. Katayama, and M. Todoki, Journal of Applied Physics **91**, 97729776 (2002), URL http://link.aip.org/link/?JAP/91/9772/1.

[23] C. Masciovecchio, G. Baldi, S. Caponi, L. Comez, S. Di Fonzo, D. Fioretto, A. Fontana, A. Gessini, S. C. Santucci, F. Sette, et al., Phys. Rev. Lett. **97**, 035501 (2006), URL http://link.aps.org/doi/10.1103/PhysRevLett.97.035501.

[24] G. Baldi, V. M. Giordano, G. Monaco, F. Sette, E. Fabiani, A. Fontana, and G. Ruocco, Phys. Rev. B **77**, 214309 (2008), URL http://link.aps.org/doi/10.1103/PhysRevB.77.214309.

[25] G. Baldi, V. M. Giordano, G. Monaco, and B. Ruta, Phys. Rev. Lett. **104**, 195501 (2010), URL http://link.aps.org/doi/10.1103/PhysRevLett.104.195501.

[26] G. Baldi, V. M. Giordano, and G. Monaco, Phys. Rev. B **83**, 174203 (2011), URL http://link.aps.org/doi/10.1103/PhysRevB.83.174203.

[27] G. Baldi, M. Zanatta, E. Gilioli, V. Milman, K. Refson, B. Wehinger, B. Winkler, A. Fontana, and G. Monaco, Phys. Rev. Lett. **110**, 185503 (2013), URL http://link.aps.org/doi/10.1103/PhysRevLett.110.185503.

[28] L. Wieczorek, H. Goldsmid, and G. Paul, in *Thermal Conductivity 20*, edited by D. Hasselman and J. Thomas, J.R. (Springer US, 1989), pp. 235–241, ISBN 978-1-4612-8069-9, URL http://dx.doi.org/10.1007/978-1-4613-0761-7_22.

[29] H. Wada and T. Kamijoh, Japanese Journal of Applied Physics **35**, L648L650 (1996), URL http://jjap.jsap.jp/link?JJAP/35/L648/.

[30] B. L. Zink, R. Pietri, and F. Hellman, Physical Review Letters **96**, 055902 (2006), URL http://link.aps.org/doi/10.1103/PhysRevLett.96.055902.

[31] B. S. W. Kuo, J. C. M. Li, and A. W. Schmid, Applied Physics A: Materials Science & Processing **55**, 289296 (1992), ISSN 0947-8396, 10.1007/BF00348399, URL http://dx.doi.org/10.1007/BF00348399.

[32] S. Moon, M. Hatano, M. Lee, and C. P. Grigoropoulos, International Journal of Heat and Mass Transfer **45**, 2439 2447 (2002), ISSN 0017-9310, URL http://www.sciencedirect.com/science/article/pii/S0017931001003477.

[33] G. Pompe and E. Hegenbarth, physica status solidi (b) **147**, 103 (1988), ISSN 1521-3951, URL http://dx.doi.org/10.1002/pssb.2221470109.

[34] D. G. Cahill, H. E. Fischer, T. Klitsner, E. T. Swartz, and R. O. Pohl, Journal of Vaccuum Science and Technology A **7**, 12591266 (1989).

[35] B. L. Zink, R. Islam, D. J. Smith, and F. Hellman, Phys. Rev. B **74**, 205209 (2006), URL http://link.aps.org/doi/10.1103/PhysRevB.74.205209.

[36] N. W. Ashcroft and N. D. Mermin, *Solid State Physics* (Saunders, Fort Worth, 1976).

[37] M. T. Dove, *Introduction to Lattice Dynamics* (Cambridge, Cambridge, 1993).

[38] J. M. Ziman, *Electrons and Phonons* (Oxford, New York, 2001).

[39] D. A. McQuarrie, *Statistical Mechanics* (University Science Books, Sausalito, 2000).

[40] J. Callaway, Physical Review **113**, 1046 (1959).

[41] P. G. Klemens, Proceedings of the Physical Society. Section A **68** (1955).

[42] P. B. Allen and J. L. Feldman, Physical Review B **48**, 1258112588 (1993).

[43] J. K. Flicker and P. L. Leath, Phys. Rev. B **7**, 22962305 (1973), URL http://link.aps.org/doi/10.1103/PhysRevB.7.2296.

[44] A. Alam and A. Mookerjee, Phys. Rev. B **72**, 214207 (2005), URL http://link.aps.org/doi/10.1103/PhysRevB.72.214207.

[45] D. Cahill and R. Pohl, Annual Review of Physical Chemistry **39**, 93121 (1988).

[46] D. G. Cahill, S. K. Watson, and R. O. Pohl, Phys. Rev. B **46**, 61316140 (1992), URL http://link.aps.org/doi/10.1103/PhysRevB.46.6131.

[47] C. Kittel, Physical Review **75**, 974 (1949).

[48] J. Larkin and A. McGaughey, Journal of Applied Physics (2013).

[49] G. C. Sosso, D. Donadio, S. Caravati, J. Behler, and M. Bernasconi, Phys. Rev. B **86**, 104301 (2012), URL http://link.aps.org/doi/10.1103/PhysRevB.86.104301.

[50] Y. He, D. Donadio, and G. Galli, Applied Physics Letters **98**, 144101 (2011), URL http://link.aip.org/link/?APL/98/144101/1.

[51] A. J. H. McGaughey and M. Kaviany, International Journal of Heat and Mass Transfer **47**, 17831798 (2004).

[52] J. D. Gale and A. L. Rohl, Molecular Simulation **29**, 291 (2003).

[53] G. T. Barkema and N. Mousseau, Phys. Rev. B **62**, 49854990 (2000), URL http://link.aps.org/doi/10.1103/PhysRevB.62.4985.

[54] F. H. Stillinger and T. A. Weber, Physical Review B **31**, 52625271 (1985).

[55] M. Durandurdu and D. A. Drabold, Phys. Rev. B **66**, 155205 (2002), URL http://link.aps.org/doi/10.1103/PhysRevB.66.155205.

[56] N. Bernstein, J. L. Feldman, and M. Fornari, Phys. Rev. B **74**, 205202 (2006), URL http://link.aps.org/doi/10.1103/PhysRevB.74.205202.

[57] K. Momma and F. Izumi, Journal of Applied Crystallography **41**, 653658 (2008), URL http://dx.doi.org/10.1107/S0021889808012016.

[58] S. Plimpton, Journal of Computational Physics **117**, 1 19 (1995), ISSN 0021-9991, URL http://www.sciencedirect.com/science/article/pii/S002199918571039X.

[59] M. L. Williams and H. J. Maris, Phys. Rev. B **31**, 45084515 (1985), URL http://link.aps.org/doi/10.1103/PhysRevB.31.4508.

[60] D. Donadio and G. Galli, Phys. Rev. Lett. **102**, 195901 (2009).

[61] Y. M. Beltukov, V. I. Kozub, and D. A. Parshin, Phys. Rev. B **87**, 134203 (2013), URL http://link.aps.org/doi/10.1103/PhysRevB.87.134203.

[62] P. B. Allen, J. L. Feldman, J. Fabian, and F. Wooten, Philosophical Magazine B **79**, 17151731 (1999).

[63] N. L. Green, D. Kaya, C. E. Maloney, and M. F. Islam, Physical Review E **83**, 051404 (2011), URL http://link.aps.org/doi/10.1103/PhysRevE.83.051404.

[64] S. Volz and G. Chen, Physical Review B **61**, 26512656 (2000).

[65] J. L. Feldman, Journal of Non-Crystalline Solids **307310**, 128 (2002), ISSN 0022-3093, URL http://www.sciencedirect.com/science/article/pii/S0022309302014503.

[66] B. Ruzicka, T. Scopigno, S. Caponi, A. Fontana, O. Pilla, P. Giura, G. Monaco, E. Pontecorvo, G. Ruocco, and F. Sette, Phys. Rev. B **69**, 100201 (2004), URL http://link.aps.org/doi/10.1103/PhysRevB.69.100201.

[67] S. N. Taraskin and S. R. Elliott, EPL (Europhysics Letters) **39**, 37 (1997), URL http://stacks.iop.org/0295-5075/39/i=1/a=037.

[68] J. Horbach, W. Kob, and K. Binder, The European Physical Journal B - Condensed Matter and Complex Systems **19**, 531 (2001), ISSN 1434-6028, URL http://dx.doi.org/10.1007/s100510170299.

[69] R. Biswas, A. M. Bouchard, W. A. Kamitakahara, G. S. Grest, and C. M. Soukoulis, Phys. Rev. Lett. **60**, 22802283 (1988), URL http://link.aps.org/doi/10.1103/PhysRevLett.60.2280.

[70] L. E. Silbert, A. J. Liu, and S. R. Nagel, Phys. Rev. E **79**, 021308 (2009), URL http://link.aps.org/doi/10.1103/PhysRevE.79.021308.

[71] J. C. Duda, T. S. English, D. A. Jordan, P. M. Norris, and W. A. Soffa, Journal of Physics: Condensed Matter **23**, 205401 (2011), URL http://stacks.iop.org/0953-8984/23/i=20/a=205401.

[72] T. Hori, T. Shiga, and J. Shiomi, Journal of Applied Physics **113**, 203514 (2013), URL http://link.aip.org/link/?JAP/113/203514/1.

[73] A. J. C. Ladd, B. Moran, and W. G. Hoover, Physical Review B **34**, 50585064 (1986).

[74] A. J. H. McGaughey and M. Kaviany, Physical Review B **69**, 094303 (2004).

[75] J. E. Turney, E. S. Landry, A. J. H. McGaughey, and C. H. Amon, Phys. Rev. B **79**, 064301 (2009), URL http://link.aps.org/doi/10.1103/PhysRevB.79.064301.

[76] J. M. Larkin, J. E. Turney, A. D. Massicotte, C. H. Amon, and A. J. H. McGaughey, to appear in Journal of Computational and Theoretical Nanoscience (2012).

[77] Y. He, D. Donadio, and G. Galli, Nano Letters **11**, 3608\textbackslashtextbackslashtextbackslashtextbackslash963611 (2011).

[78] V. Martin-Mayor, M. Mezard, G. Parisi, and P. Verrocchio, The Journal of Chemical Physics **114**, 8068 (2001), URL http://link.aip.org/link/?JCP/114/8068/1.

[79] P. Sheng and M. Zhou, Science **253**, 539542 (1991), URL http://www.sciencemag.org/

content/253/5019/539.abstract.

[80] V. Mazzacurati, G. Ruocco, and M. Sampoli, EPL (Europhysics Letters) **34**, 681 (1996), URL http://stacks.iop.org/0295-5075/34/i=9/a=681.

[81] S. R. Bickham and J. L. Feldman, Phys. Rev. B **57**, 1223412238 (1998), URL http://link.aps.org/doi/10.1103/PhysRevB.57.12234.

[82] S. R. Bickham, Phys. Rev. B **59**, 48944897 (1999), URL http://link.aps.org/doi/10.1103/PhysRevB.59.4894.

[83] J. Fabian and P. B. Allen, Phys. Rev. Lett. **77**, 38393842 (1996), URL http://link.aps.org/doi/10.1103/PhysRevLett.77.3839.

[84] J. Fabian, J. L. Feldman, C. S. Hellberg, and S. M. Nakhmanson, Phys. Rev. B **67**, 224302 (2003), URL http://link.aps.org/doi/10.1103/PhysRevB.67.224302.

[85] N. Xu, V. Vitelli, M. Wyart, A. J. Liu, and S. R. Nagel, Phys. Rev. Lett. **102**, 038001 (2009), URL http://link.aps.org/doi/10.1103/PhysRevLett.102.038001.

[86] V. Vitelli, N. Xu, M. Wyart, A. J. Liu, and S. R. Nagel, Phys. Rev. E **81**, 021301 (2010), URL http://link.aps.org/doi/10.1103/PhysRevE.81.021301.

[87] G. Ruocco, F. Sette, R. Di Leonardo, G. Monaco, M. Sampoli, T. Scopigno, and G. Viliani, Phys. Rev. Lett. **84**, 57885791 (2000), URL http://link.aps.org/doi/10.1103/PhysRevLett.84.5788.

[88] J. Shiomi, K. Esfarjani, and G. Chen, Physical Review B **84**, 125209 (2011).

[89] K. Esfarjani, G. Chen, and H. T. Stokes, Physical Review B **84**, 085204 (2011).

[90] D. P. Sellan, J. E. Turney, A. J. H. McGaughey, and C. H. Amon, Journal of Applied Physics **108**, 113524 (2010).

[91] Y. H. Lee, R. Biswas, C. M. Soukoulis, C. Z. Wang, C. T. Chan, and K. M. Ho, Phys. Rev. B **43**, 65736580 (1991), URL http://link.aps.org/doi/10.1103/PhysRevB.43.6573.

[92] M. S. Love and A. C. Anderson, Phys. Rev. B **42**, 18451847 (1990), URL http://link.aps.org/doi/10.1103/PhysRevB.42.1845.

[93] S. Li, Y. Jiang, Z. Wu, J. Wu, Z. Ying, Z. Wang, W. Li, and G. J. Salamo, Applied Surface Science **257**, 8326 (2011), ISSN 0169-4332, URL http://www.sciencedirect.com/science/article/pii/S0169433211004715.

[94] J. L. Feldman, N. Bernstein, D. A. Papaconstantopoulos, and M. J. Mehl, Phys. Rev. B **70**, 165201 (2004), URL http://link.aps.org/doi/10.1103/PhysRevB.70.165201.

[95] M. E. Siemens, Q. Li, R. Yang, K. A. Nelson, E. H. Anderson, M. M. Murnane, and H. C. Kapteyn, Nature Materials **9**, 2630 (2010).

[96] G. A. Slack (Academic Press, 1979), vol. 34 of *Solid State Physics*, p. 1 71, URL http://www.sciencedirect.com/science/article/pii/S0081194708603598.

[97] R. O. Pohl, X. Liu, and E. Thompson, Rev. Mod. Phys. **74**, 9911013 (2002), URL http://link.aps.org/doi/10.1103/RevModPhys.74.991.

[98] W. Schirmacher, EPL (Europhysics Letters) **73**, 892 (2006), URL http://stacks.iop.org/0295-5075/73/i=6/a=892.

[99] W. Schirmacher, G. Ruocco, and T. Scopigno, Phys. Rev. Lett. **98**, 025501 (2007), URL http://link.aps.org/doi/10.1103/PhysRevLett.98.025501.